4-2018

Neonatal Subventricular Zone Neural Stem Cells Release Extracellular Vesicles that Act as a Microglial Morphogen

Mary C. Morton
Clemson University

Victoria N. Neckles
Clemson University

Caitlin M. Seluzicki
Clemson University

Jennie C. Holmberg
Clemson University

David M. Feliciano
Clemson University, dfelici@clemson.edu

Article

Cell Reports

Neonatal Subventricular Zone Neural Stem Cells Release Extracellular Vesicles that Act as a Microglial Morphogen

Graphical Abstract

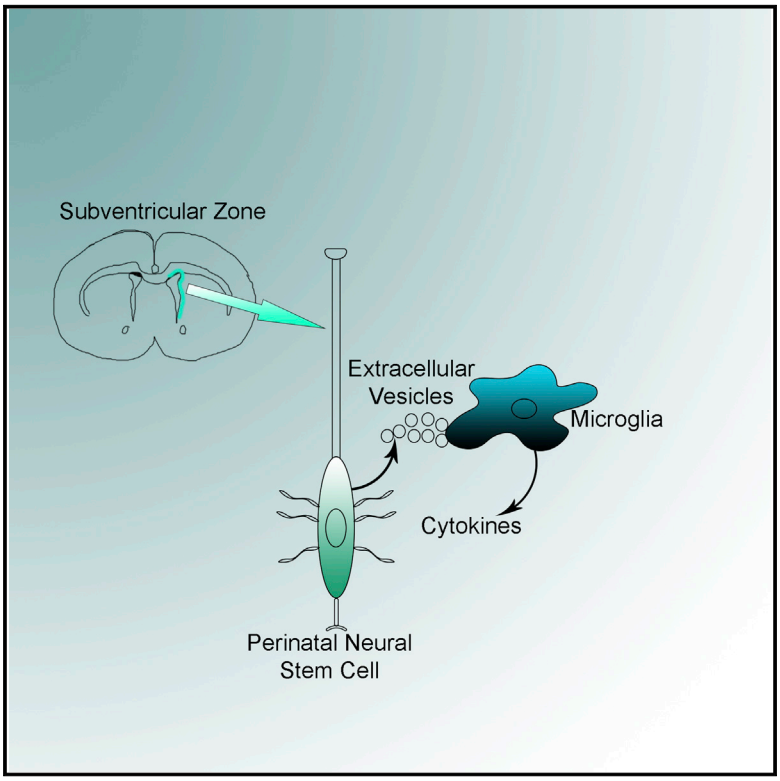

Authors

Mary C. Morton, Victoria N. Neckles, Caitlin M. Seluzicki, Jennie C. Holmberg, David M. Feliciano

Correspondence

dfelici@clemson.edu

In Brief

Morton et al. demonstrate that neonatal subventricular zone neural stem cells release extracellular vesicles. A combination of primary stem cell culture, *in vivo* genetic manipulations, next-generation small RNA sequencing, and neonatal extracellular vesicle transplantations reveal that extracellular vesicles are transferred to and regulate microglia in the neonatal brain.

Highlights

- Neonatal SVZ neural stem cells release extracellular vesicles
- SVZ neural stem cell extracellular vesicles are targeted to microglia
- Neural stem cell extracellular vesicles and RNA content regulate microglia morphology

Data and Software Availability

GSE110892

Morton et al., 2018, Cell Reports *23*, 78–89
April 3, 2018
https://doi.org/10.1016/j.celrep.2018.03.037

CellPress

OPEN ACCESS
CellPress

Cell Reports
Article

Neonatal Subventricular Zone Neural Stem Cells Release Extracellular Vesicles that Act as a Microglial Morphogen

Mary C. Morton,[1] Victoria N. Neckles,[1] Caitlin M. Seluzicki,[1] Jennie C. Holmberg,[1] and David M. Feliciano[1,2,*]
[1]Department of Biological Sciences, Clemson University, Clemson, SC 29634-0314, USA
[2]Lead Contact
*Correspondence: dfelici@clemson.edu
https://doi.org/10.1016/j.celrep.2018.03.037

SUMMARY

Subventricular zone (SVZ) neural stem cells (NSCs) are the cornerstone of the perinatal neurogenic niche. Microglia are immune cells of the nervous system that are enriched in the neonatal SVZ. Although microglia regulate NSCs, the extent to which this interaction is bi-directional is unclear. Extracellular vesicles (EVs) are cell-derived particles that encase miRNA and proteins. Here, we demonstrate that SVZ NSCs generate and release EVs. Neonatal electroporated fluorescent EV fusion proteins were released by NSCs and subsequently cleared from the SVZ. EVs were preferentially targeted to microglia. Small RNA sequencing identified miRNAs within the EVs that regulate microglia physiology and morphology. EVs induced a transition to a CD11b/Iba1 non-stellate microglial morphology. The transition accompanied a microglial transcriptional state characterized by Let-7-regulated cytokine release and a negative feedback loop that controlled NSC proliferation. These findings implicate an NSC-EV-microglia axis and provide insight to normal and pathophysiological brain development.

INTRODUCTION

Neurons are produced by stem cells that reside in discrete regions of the adult mammalian brain called neurogenic zones. The subventricular zone (SVZ) is one of two canonical neurogenic regions that produce neurons in the adult mammalian brain (Lim and Alvarez-Buylla, 2016). The renewal capacity endowed by the SVZ likely allows for continued adaptation to environmental olfactory cues by generating olfactory bulb neurons (Lledo and Valley, 2016). Mutations in SVZ neural stem cells (NSCs) make them a likely culprit in the generation of certain tumors and malformations (Dietrich et al., 2008; Vescovi et al., 2006; Zhou et al., 2011). Intercellular communication within the SVZ is paramount for producing the appropriate numbers and types of cells (Choe et al., 2015). Therefore, the identification of mechanisms by which niche homeostasis is maintained or perturbed has far-reaching implications.

Microglia are hematopoietically derived myeloid cells derived from yolk sac macrophages that function as neuro-resident immune cells (Ginhoux et al., 2010; Prinz et al., 2017). Myeloid cells invade the mid-gestation brain through the vasculature and subsequently produce ~95% of microglia during the first postnatal weeks (Alliot et al., 1991, 1999). A band of microglia is found within the SVZ during this perinatal period (Shigemoto-Mogami et al., 2014). During adulthood, this band of microglia disperses to form an evenly distributed immunological matrix within the parenchyma (Shigemoto-Mogami et al., 2014). Few studies have demonstrated that SVZ NSCs influence microglia (Pluchino and Cossetti, 2013; Sato, 2015).

Extracellular vesicles (EVs) are found throughout the developing nervous system (Morton and Feliciano, 2016). EVs are membranous particles that range in size from 50–350 nm and encapsulate microRNA (miRNA), mRNA, and proteins (Raposo and Stoorvogel, 2013). EVs are classified into two categories: exosomes and ectosomes. Exosomes are intraluminal vesicles that have been exocytosed following multivesicular body fusion with the cell membrane (Cocucci and Meldolesi, 2015). Ectosomes are larger than exosomes and are generated by outward budding of the cell membrane (Cocucci and Meldolesi, 2015). Recent studies demonstrate that SVZ-derived neural stem/precursor cells release EVs (Cossetti et al., 2014; Iraci et al., 2017). Neurosphere-derived EVs carry miRNA, mRNA, and proteins such as the interferon gamma receptor and active asparaginase (Cossetti et al., 2014; Iraci et al., 2017). Adult hypothalamic neuronal stem cells also produce exosomes that have longevity-extending properties (Zhang et al., 2017). However, the *in vivo* cellular targets of NSC EVs are unclear.

This study was performed to determine the extent to which SVZ NSCs release EVs and to identify *in vivo* NSC EV targets, if any. Neonatal SVZ NSCs were found to release EVs. Neonatal intraventricular transplanted NSC EVs were selectively taken up by microglia. NSC EV uptake was associated with a CD11b/Iba1-positive morphological shift to a reduced complexity. RNA sequencing and cytokine analysis revealed a change in the transcriptional network and cytokine profile of microglia following NSC exosome treatment.

RESULTS

Neonatal SVZ NSCs Release EVs

Primary SVZ NSCs were cultured as a monolayer from post-natal day 0 (P0) mice and subjected to immunocytochemistry for the

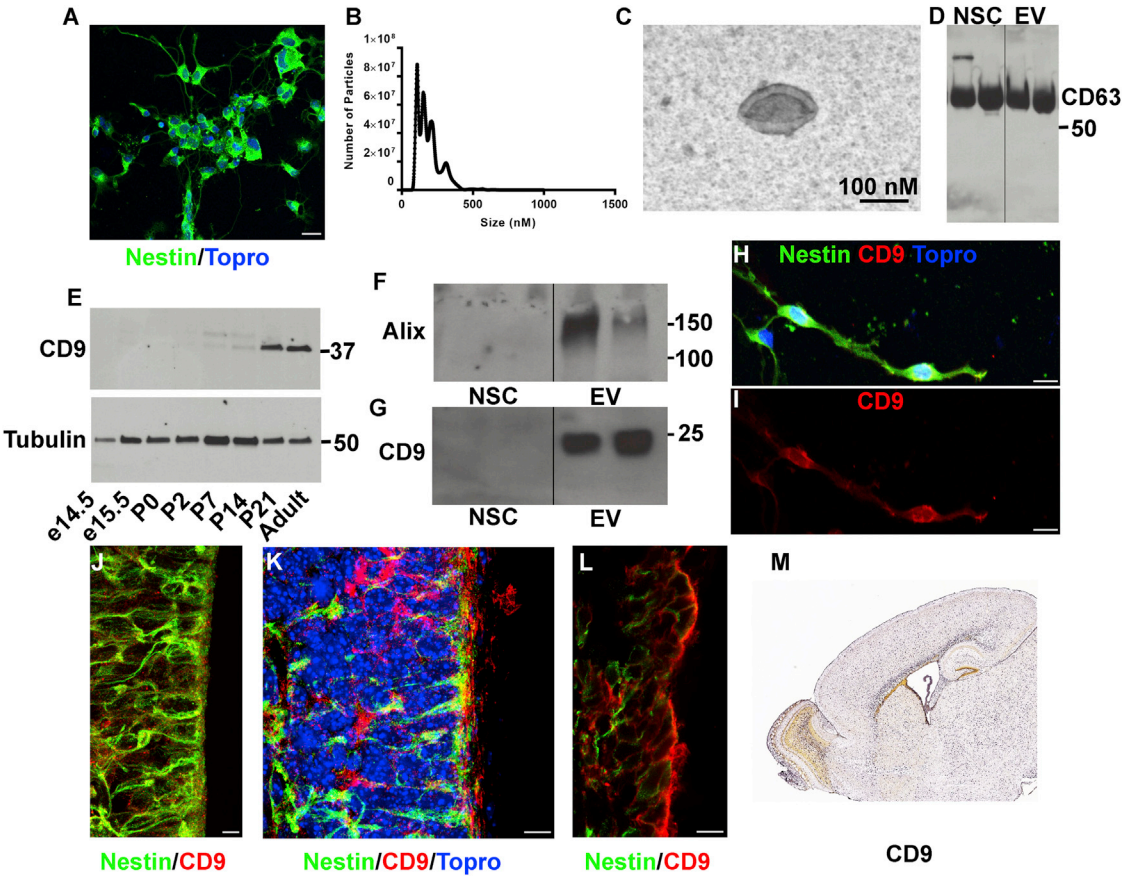

Figure 1. Neonatal SVZ NSCs Release EVs

(A) Immunocytochemistry for Nestin (green) and TO-PRO-3 (blue) in primary monolayer culture of P0 SVZ NSCs after 2 days *in vitro*. Scale bar, 25 μm.
(B) Nanosight particle profile of EVs derived from the P100 fraction of NSCs.
(C) Electron micrograph of an NSC-derived exosome. Scale bar, 100 nm.
(D) Western blot of CD63 in NSC lysate or NSC EV P100 fractions.
(E) Western blot of CD9 and β3-tubulin from dorsal forebrain extracts.
(F) Western blot for ALIX in SVZ NSC EV P100 fractions as in (D).
(G) Western blot for CD9 from NSC EV P100 fractions as in (D).
(H and I) Immunohistochemistry of Nestin (green), TO-PRO-3 (blue), CD9 (red) (H), and CD9 (I) in P0 SVZ NSC cultures. Scale bars, 12.5 μm.
(J) Nestin (green) and CD9 (red) expression within the SVZ at P0. Scale bar, 5 μm.
(K and L) Nestin (green), CD9 (red), and TO-PRO-3 (blue) within the SVZ at P4. Scale bars, 25 μm.
(M) *In situ* hybridization of CD9 in a P14 sagittal brain section from the Allen Brain Institute Developing Mouse Brain Atlas. Image credit: Allen Institute.

NSC marker protein Nestin. Neonatal SVZ cultures were double-cortin (DCX)-negative (data not shown), whereas most cells were Nestin-positive (~92%) (Figure 1A). Neonatal SVZ NSC conditioned medium was subjected to low-speed centrifugation to remove debris and dead cells, followed by nanoparticle tracking analysis. Four peaks were identified at 89, 129, 199, and 263 nm with an average size of 164.9 ± 7.2 nm. In addition to conditioned medium, we analyzed medium subjected to an ultracentrifugation EV enrichment protocol. This NSC P100 fraction contained four peaks at 109, 154, 209, and 312 nm with an average size of 190.7 ± 5.2 nm (Figure 1B). EVs were also extracted using polymer precipitation and had an average size of 167.0 ± 3.8 nm (data not shown). NSC EV size was confirmed by electron microscopy and confirmed to have an exosome morphology (Figure 1C). CD63, an EV marker protein, was confirmed to be expressed in NSCs and EVs (Figure 1D). Another EV protein, CD9, was detected in dorsal forebrain extracts. CD9 was present in the neonatal brain and upregulated by P7 (Figure 1E). CD9 was detected in primary neonatal SVZ NSC EVs by western blot (Figure 1F). Moreover, ALIX, an exosome cargo protein, was present in SVZ NSC EVs (Figure 1G). CD9 expression was further confirmed in primary SVZ NSC cultures by immunocytochemistry (Figures 1H and 1I). CD9 was present within the processes of SVZ NSCs and was peri-nuclear, consistent with a previous report (Llorens-Bobadilla et al., 2015). To examine CD9 protein expression *in vivo*, immunohistochemistry was performed on P0 and P4 brains. CD9 expression was present along the ventricular wall in Nestin-positive NSCs at P4 (Figures 1J–1L). The enrichment of CD9 within the neonatal SVZ was consistent with *in situ* hybridizations of sagittal sections from the

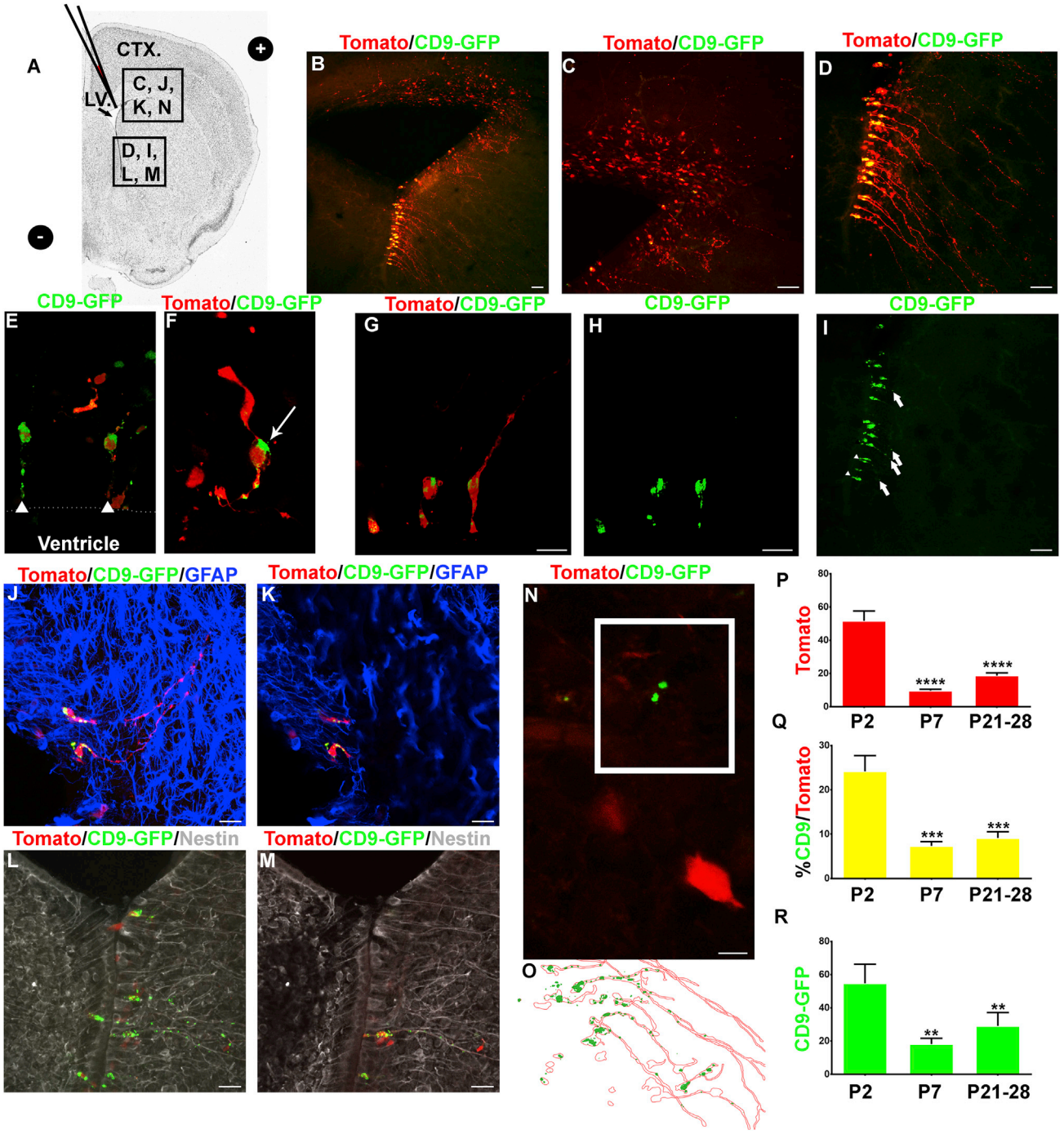

Figure 2. SVZ NSCs Release CD9 *In Vivo*

(A) Schematic diagram of a coronal section, indicating the direction of electrodes used for neonatal electroporation; black rectangles indicate the corresponding regions imaged. Image credit: Allen Institute.

(B) 5× image of the SVZ of a P2 mouse following P0 electroporation with Tomato (red) and CD9-GFP (green). Scale bar, 100 μm.

(C) 20× image of the dorsolateral SVZ from (B). Scale bar, 50 μm.

(D) 20× image of the ventro-lateral SVZ from (B). Scale bar, 50 μm.

(E–H) 63× images of SVZ NSCs electroporated with Tomato (red) and CD9-GFP (green) demonstrating differences in CD9-GFP localization in apical and basal processes (E) and soma (F). Note the distribution of Tomato and CD9-GFP (G, merge) and CD9-GFP alone (H). Scale bars, 50 μm.

(I) CD9-GFP distribution in relation to the Tomato-positive SVZ NSC soma located at the ventricle. Arrows point to CD9-GFP in the basal fiber, and arrowheads point to apical fibers with CD9-GFP present. Scale bar, 50 μm.

(legend continued on next page)

Allen Brain Institute (Figure 1M; Henry and Hohmann, 2012). These results confirm that neonatal SVZ NSCs release EVs *in vitro*.

SVZ NSCs Release CD9 *In Vivo*

N2a cells were transfected with CD9-GFP- and Tomato (fluorescent protein)-encoding DNA (Figure S1A). CD9-GFP exhibited a cytoplasmic distribution in N2a cells and could be detected in extracellular vesicle and exosome fractions from sucrose gradients along with ALIX, CD63, and a His tag present within CD9-GFP (Figure S1B). Approximately 47% (n = 9, 46.59 ± 4.943) of CD9-GFP particles were extracellular, consistent with the hypothesized release of CD9 (Figure S1C). N2a CD9-GFP exosomes incubated with naive N2a cultures were detected surrounding, but not within, N2a nuclei (Figure S1D). CD9-GFP uptake in N2a cells was confirmed in cells transfected with Tomato plasmids (Figure S1E). Time-lapse imaging demonstrated considerable movement of intracellular CD9-GFP (Figure S1F). The release of CD9-GFP was confirmed by live imaging (Figure S1G).

To study NSC exosomes, Tomato fluorescent protein- and CD9-GFP-encoding plasmids were electroporated into the SVZ of P0 mice, and NSCs were examined (Figure 2A). Expression of Tomato fluorescent protein was detected throughout the soma (Figures 2B–2D). CD9-GFP-positive cells were most frequent along the ventro-lateral ventricular wall (Figures 2B–2D). CD9-GFP was detected within cells with a B1-like NSC morphology (Figures 2E–2H). CD9-GFP localized to the apical and basal processes (Figures 2E and 2I). Cells with an NSC morphology stained positively for glial fibrillary acid protein (GFAP) by P7 (Figures 2J and 2K). B1-like tomato/CD9-GFP-positive cells were also Nestin-positive, confirming their identity as NSCs (Figures 2L and 2M). CD9-GFP was detected outside of electroporated cells (Figures 2N and 2O).

We detected ~52 Tomato-positive cells/SVZ 48 hr post-electroporation (Figure 2P). Tomato-positive cells remaining in the SVZ significantly decreased by 80% from P2–P7 (Figure 2P). This result is consistent with the prevailing notion that NSCs generate transit-amplifying cells that produce neuroblasts and migrate away from the SVZ to the olfactory bulb (OB). Similar to transient thymidine labeling (for example, bromodeoxyuridine [BrdU]), DNA plasmids are diluted from dividing NSCs. NSCs were co-electroporated with either of two CD9-GFP plasmids that had cytomegalovirus (CMV) or CAG promoters. CD9-GFP expression was limited to 7.52% (CMV) and 24% (CAG) of Tomato-positive cells in the SVZ. CAG-CD9-GFP was co-expressed more frequently than CMV-CD9-GFP in Tomato-positive cells, which was not surprising given that CAG-CD9-GFP was generated by cloning it into the Tomato plasmid. CAG-CD9-GFP was therefore used for quantification. The percentage of cells co-expressing CD9-GFP and Tomato significantly decreased from 24% to 7.32% at P7 (Figure 2Q). The reduction in the percentage of CD9-GFP/Tomato co-expressing cells was similar in P21–P28 brains.

When considering the reduction of Tomato-positive cells, and consistent with Tomato/CD9-GFP double-positive cells, these results support a model for which 71% of CD9-GFP/Tomato-positive cells are NSCs. This is likely an underestimate because NSCs also generate ependyma and quiescent NSCs that remain in the SVZ. For every electroporated cell 48 hr post-electroporation, at least one extracellular particle could be detected (54.77 CD9-GFP particles/image) (Figure 2R). The number of CD9-GFP particles outside of co-electroporated Tomato NSCs decreased by 7 days post-electroporation to 18.20 particles and remained similar (19.06) in P21–P28 mice (Figure 2R). These results demonstrate that SVZ NSCs release CD9, which is subsequently cleared from the extracellular milieu.

SVZ NSCs Selectively Target Microglia

It was tempting to speculate that the commensurate reduction of extracellular CD9 was consistent with a model in which NSC EVs were targeted for removal. The fact that extracellular CD9-GFP-positive particles were released and decreased over time could reflect a passive or active clearing process. An influx of microglia into the neonatal SVZ occurs contemporaneously with the loss of CD9-GFP. We therefore hypothesized that active clearing by microglia might be responsible for the loss in total number of CD9-GFP-positive particles. Microglia express the ionized calcium-binding adaptor molecule 1 (Iba1). We found that Iba1-positive microglia co-localized with extracellular CD9-GFP from neonatal SVZ electroporations (Figures 3A and 3B). As an initial experiment, to perform a more unbiased assessment, N2a exosomes from CD9-GFP-transfected cells were labeled with the fluorescent lipophilic dye DiI (1,1'-Dioctadecyl-3,3,3′,3′-Tetramethylindocarbocyanine Perchlorate). Exosomes were then injected intraventricularly into the lateral ventricles of neonatal mice (Figure 3C). One to seven days after injection, mice were harvested, and brains were isolated. A population of cells near the lateral ventricles were labeled with DiI and GFP (Figures 3D–3E). Cells occasionally had a stellate morphology reminiscent of microglia (Figure 3F). Staining with Iba1 confirmed the identity of these cells as microglia (Figure 3F). Approximately

(J) SVZ from a Tomato-electroporated (red) and CD9-GFP-electroporated (green) mouse stained for GFAP (blue). Scale bar, 25 μm.
(K) Individual Z section from (J). Scale bar, 25 μm.
(L) 20× image of a CD9-GFP-electroporated (green) and Tomato-electroporated (red) brain stained for Nestin (white). Scale bar, 25 μm.
(M) Individual Z section from (L). Scale bar, 25 μm.
(N) 63× zoom-2 image within the SVZ of Tomato-electroporated (red) and CD9-GFP-electroporated (green) mice showing extracellular CD9-GFP-positive particles. Scale bar, 5 μm.
(O) A tracing of an individual slice showing a Tomato-positive cell body (red) and CD9-GFP (green).
(P) Quantification of the number of Tomato-positive SVZ cells from P2–P28.
(Q) Quantification of CD9-GFP and Tomato-positive cells in the SVZ from P2–P28.
(R) Quantification of the number of extracellular CD9-GFP-positive particles in the SVZ from P2–P28.
See also Figure S1. Data are represented as mean ± SEM. **p < 0.01, ***p < 0.001, ****p < 0.0001.

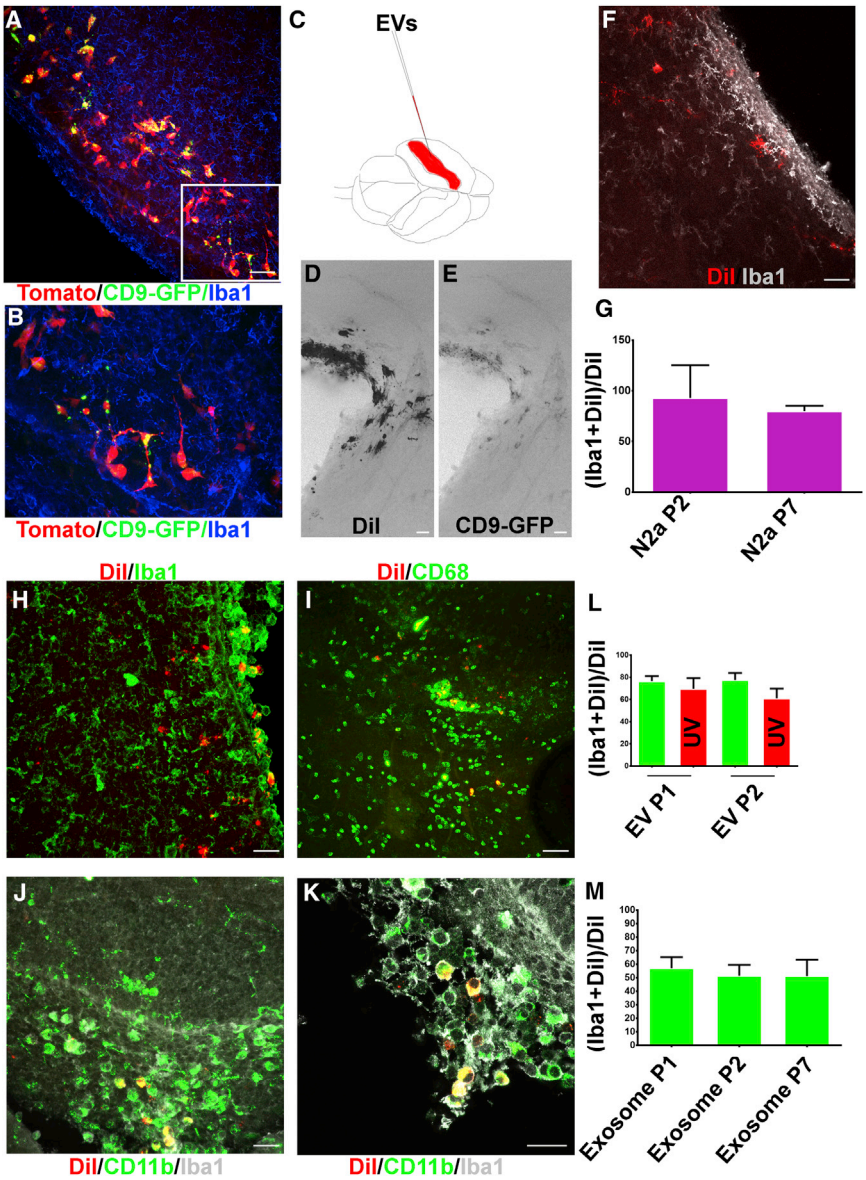

Figure 3. NSC EVs Selectively Target Microglia

(A) 20× image showing Iba1-positive microglia (blue) in proximity to Tomato-electroporated (red) cells and CD9-GFP-positive particles (green). Scale bar, 50 μm.

(B) 20× image of (A).

(C) Schematic of EV transplantations.

(D and E) DiI (D) and CD9-GFP (E, green) fluorescence within the SVZ of P7 brains following CD9-GFP N2a EV transplantation. Scale bar, 50 μm.

(F) Brain transplanted with DiI-labeled EVs (red) and stained for the microglia marker Iba1 (white). Scale bar, 50 μm.

(G) Quantification of co-localization of Iba1 and DiI following N2a transplantations and analysis at P2 and P7.

(H) 20× image of a lateral SVZ following primary NSC DiI-labeled EV (red) transplantation stained for Iba1 (green). Scale bar, 50 μm.

(I) 20× image of a dorso-lateral SVZ following primary NSC DiI-labeled EV (red) transplantation stained for CD68 (green). Scale bar, 50 μm.

(J and K) 20× (J) and 63× (K) image of SVZ following primary NSC DiI-labeled EV (red) transplantation stained for CD11b (green) and Iba1 (white). Scale bars, 25 μm.

(L) Quantification of Iba1 co-localized EVs without (green) or with (red) UV treatment from NSC EV transplantations.

(M) Quantification of the number of Iba1-positive, DiI-positive cells in the SVZ from P1–P7 from NSC exosome transplantations.

Data are represented as mean ± SEM.

93% (92.84 ± 32.44, n = 8) of DiI exosomes co-localized with microglia at P2 and 80% at P7 (79.77 ± 5.448, n = 14) (Figure 3G). Because N2a cells are derived from a mouse tumor, we wondered to what extent these results reflected and were consistent with NSC-derived EVs. Therefore, NSCs from P0 mouse brains were cultured. SVZ NSC EVs from P100 fractions were labeled with DiI and injected into P0 mice. NSC EVs were predominantly targeted to Iba1-positive microglia (Figure 3H). EV-labeled microglia often had a rounded appearance and were frequently contiguous with the lateral ventricles and SVZ. CD68 and CD11b are two markers of microglia that are expressed in neonatal SVZ microglia. Consistent with these findings, DiI-labeled cells were double-positive for CD68 and Iba1 as well as CD11b and Iba1 (Figures 3I–3K). The majority of NSC EV P100-labeled cells were Iba1-positive microglia (control 24 hr = 76.52 ± 4.608, UV-treated 24 hr = 69.64 ± 9.661, control 48 hr = 77.57 ± 6.263, UV-treated 48 hr = 61 ± 8.860) (Figure 3L). Because internal nucleic acid content is proposed to be transferred to and modify recipient cells, EVs were subjected to UV treatment, but no significant change in Iba1 co-localization was documented (Figure 3L). Exosomes were further isolated from SVZ NSC EVs and transplanted into neonates. Iba1-positive microglia accounted for more than half of all exosome-labeled cells (P1 = 57.07 ± 8.134, P2 = 51.46 ± 7.996, P7 = 51.28 ± 12.13) (Figure 3M). The percentage of incorporation is not simply because microglia represent 50% of the total number of cells in the SVZ. Although the quantity of microglia fluctuates over time, microglia account for 4%–10% of total cells in the SVZ (Shigemoto-Mogami et al., 2014). This number is substantially less than the exosome uptake by microglia. Taken together, SVZ NSC exosomes selectively label microglia.

SVZ NSC EVs Act as a Microglial Morphogen

The appearance of microglia in the SVZ coincided with the release and uptake of NSC EVs. To identify the functional effects of EVs on microglia, small RNA sequencing was performed. RNA sequencing identified numerous miRNAs in NSC P100 EVs, and we considered the most abundant

miRNAs having reads 10-fold greater than the average miRNA (Figure 4A). miR-9, Let-7, miR-26, and miR-181 were highly enriched in NSC EVs. Members from each of these families have roles in regulating microglia morphology and physiology (Kumar et al., 2015; Lehmann et al., 2012; Yao et al., 2014; Zhang et al., 2015). Based on these results, it was hypothesized that EVs regulate CD11b-positive microglia to induce a rounded non-stellate phenotype (Figure 4B). We noted that, in comparison with the contralateral hemisphere, NSC P100 EV transplantation increased CD11b-positive microglia (Figures 4C and 4D). UV pre-treatment of EVs resulted in fewer CD11b-positive microglia in comparison with control SVZ NSC EVs (Figure 4E). 24 hr post-transplantation, labeled microglia were found grasping the ventricle, contiguous with and on the apical portion of the lateral ventricular wall or in clusters within the choroid plexus. Microglia within the ventricle or choroid were often CD11b-positive and rounded, having an average ellipticity of 0.64; in comparison, unlabeled CD11b-positive microglia were more stellate, with a lower ellipticity of 0.36 (Figure 4F). Because EVs induced CD11b microglia and because CD11b was more frequently associated with a rounded morphology, microglia morphology was analyzed following NSC EV treatment. Microglia generate filopodium-like processes that survey the extracellular environment (Nimmerjahn et al., 2005). The number of processes was quantified in Iba1-positive microglia. In comparison with non-labeled cells within the same slice, NSC EV-labeled microglia were less complex and this phenotype persisted up to 7 days (Figure 4G). SVZ NSC exosome-labeled microglia also had a reduced complexity that was reversed by UV pre-treatment (Figure 4H). Based on these experiments, the content of NSC exosomes appeared to be important for the morphological changes of microglia. Because several members of the Let-7 family were the most abundant and frequently identified EV miRNAs, we hypothesized that exosomal Let-7 might regulate microglia morphology. Exosomes from N2a cells transfected with a Let-7 sponge were collected. Exosomes were subjected to mock or synthetic Let-7 transfections and transplanted into the SVZ of neonatal mice. Synthetic Let-7 miRNA-transfected exosomes induced microglia to acquire a rounder appearance that differed from the mock-transfected exosomes (Figures 4I–4L). These results confirm that SVZ NSCs release exosomes that are targeted to, taken up by, and modify microglia.

NSC EVs Activate a Microglia Transcriptional Network, Resulting in an NSC Feedback Loop

Next-generation RNA sequencing was performed to gain mechanistic insight into how EVs modify microglia. Microglia treated with NSC EVs had 1,713 transcripts that were upregulated greater than 2-fold (Figure 5A). 1,175 were significantly downregulated by greater than 2-fold (Figure 5A). Gene ontology analysis revealed that immune system processes and inflammatory responses were the most highly enriched and significantly represented terms (Figure 5B). Examination of transcripts within heatmaps indicated that the most highly upregulated transcripts included cytokines such as interleukin-1α (IL-1α), IL-1β, and IL-6 (Figure 5C). In agreement, network analysis of the top differentially regulated transcripts included a cytokine node at the core of this network (Figure 5D). Upregulation of cytokines was unbiasedly validated in microglia-conditioned medium (Figure 5E). Exosome treatments were sufficient to upregulate cytokines, and we found no evidence that the effect was due to cytokines present within the EVs (data not shown). The regulation of cytokines is likely dependent on NSC exosome content. Because Let-7 members were the most prevalent miRNAs detected and because Let-7 has been shown to activate the endosomal TLR-7 receptor, we hypothesized that Let-7 family members may modulate the transcriptional response that induces cytokines. To test this hypothesis, plasmids expressing Let-7 sponges were transfected into N2a cells, and then synthetic Let-7 miRNAs were transfected into EVs. EVs were then added to microglia, and cytokine responses were measured. Synthetic Let-7-containing EVs stimulated robust release of cytokines from microglia that mimicked the effect of NSC EVs (Figure 5F). SVZ NSC EVs induced a minor response from RAW 264.7 macrophages that differed from microglia (Figure S2). For example, macrophages released IL-1α, IL-6, and granulocyte-colony stimulating factor (G-CSF). In contrast, G-CSF was not increased for microglia, whereas IL-1β was not stimulated in macrophages after NSC EV treatment. We hypothesized that the release of factors from microglia following exosome uptake may exert a feedback response to SVZ NSCs. To test this hypothesis, and as a test of the functional significance of NSC exosome uptake by microglia, conditioned medium from non-treated or EV-treated microglia was injected back into the lateral ventricles of P0 mice, and EdU (5-ethynyl-2'-deoxyuridine) labeling was performed (Figure 5G). Conditioned medium from microglia treated with exosomes, but not control microglia, reduced the number of dividing NSCs (Figure 5H). Taken together, these results demonstrate a robust and significant effect of exosomes on microglia signaling that forms a negative feedback loop to NSCs during the neonatal period.

DISCUSSION

Here evidence is provided that EVs are released from neonatal SVZ NSCs and subsequently taken up by microglia. Primary SVZ NSCs released EVs, as determined by nanosight particle tracking analysis and western blotting for EV marker proteins. Of the EV proteins, CD9 was found to be co-localized *in vivo* and *in vitro* with Nestin-positive NSCs. These results are consistent with the well-documented expression of CD9 in stem and stem-like cells (Karlsson et al., 2013; Kolle et al., 2009; Leung et al., 2011; Llorens-Bobadilla et al., 2015; Oka et al., 2002; Shi et al., 2017; Terada et al., 2002). A recent study demonstrated CD9 expression within adult SVZ NSCs (Llorens-Bobadilla et al., 2015). CD9 is also widely reported to be released with EVs, including from N2a cells.

Cerebrospinal fluid (CSF) contains EVs that are present during perinatal brain development (Feliciano et al., 2014; Tietje et al., 2014). To determine whether NSCs may generate EVs, neonatal electroporations of CD9-GFP were performed. Extracellular CD9-GFP was found within 48 hr after electroporation. Previous studies have also reported the release of particles during neurogenesis that correlate with different developmental processes,

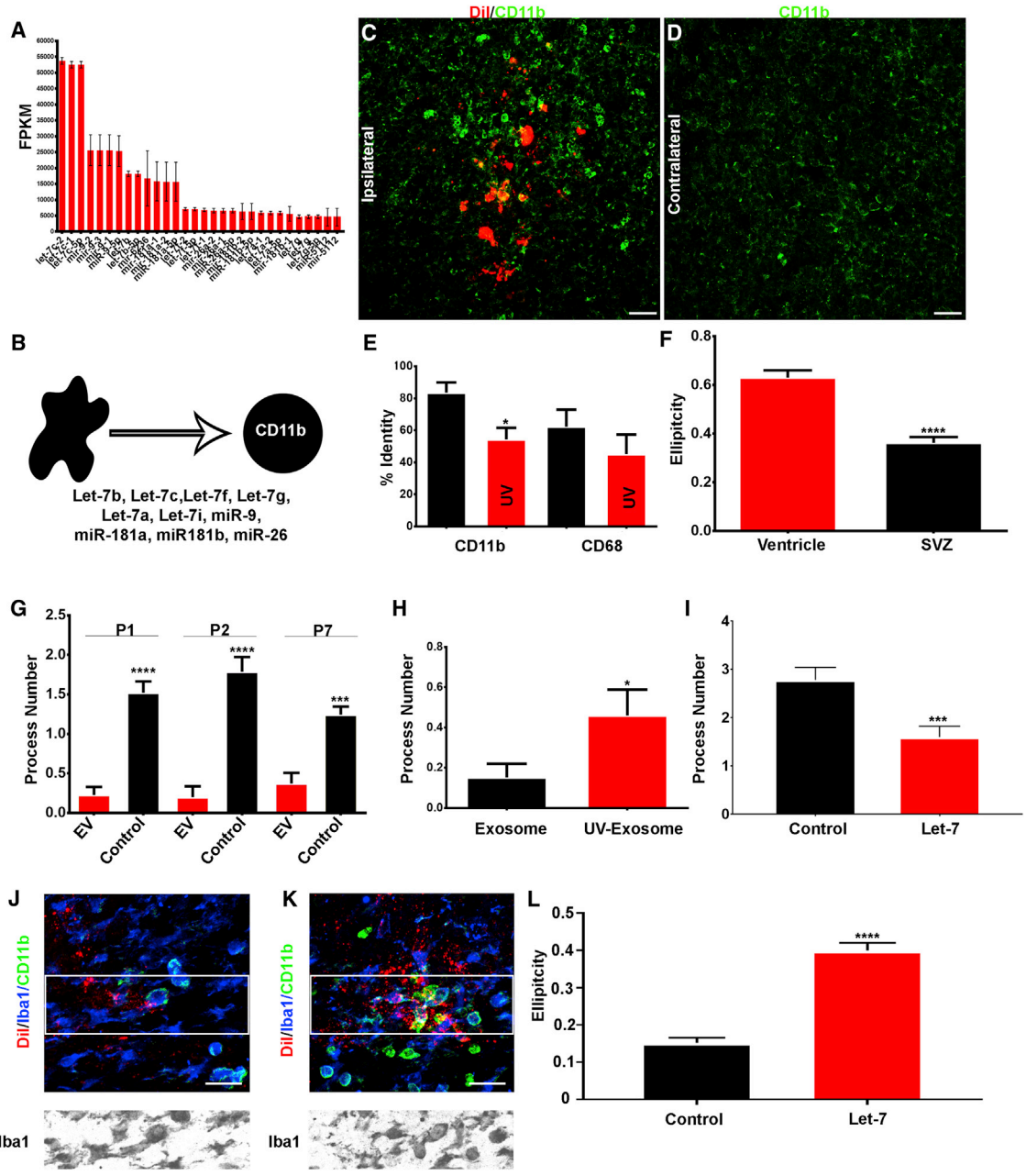

Figure 4. NSC EVs Act as a Microglial Morphogen

(A) Identity and quantity of NSC EV miRNAs.

(B) Schematic of predicted NSC EV miRNA functions.

(C and D) Image demonstrating CD11b-labeled (green) cells in DiI-labeled EV-transplanted (red) ipsilateral (C) or contralateral (D) hemispheres. Scale bar, 25 μm.

(E) Quantification of the percentage of CD11b- or CD68-positive microglia.

(F) Measurement of regional microglia ellipticity.

(G) Average number of cellular processes in Iba1-positive microglia following EV transplantation.

(H) Quantification of the number of cellular processes in Iba1-positive microglia labeled by control or UV pre-treated NSC exosomes.

(I) Quantification of the number of cellular processes following treatment with control N2a exosomes or N2a exosomes packaged with synthetic Let-7.

(J and K) Representative images of control (J) or Let-7 (K) EV transplantations from (I). Scale bars, 50 μm.

(L) Quantification of microglia ellipticity following control or Let-7 exosome uptake.

Data are represented as mean ± SEM. *p < 0.05, ***p < 0.001, ****p < 0.0001.

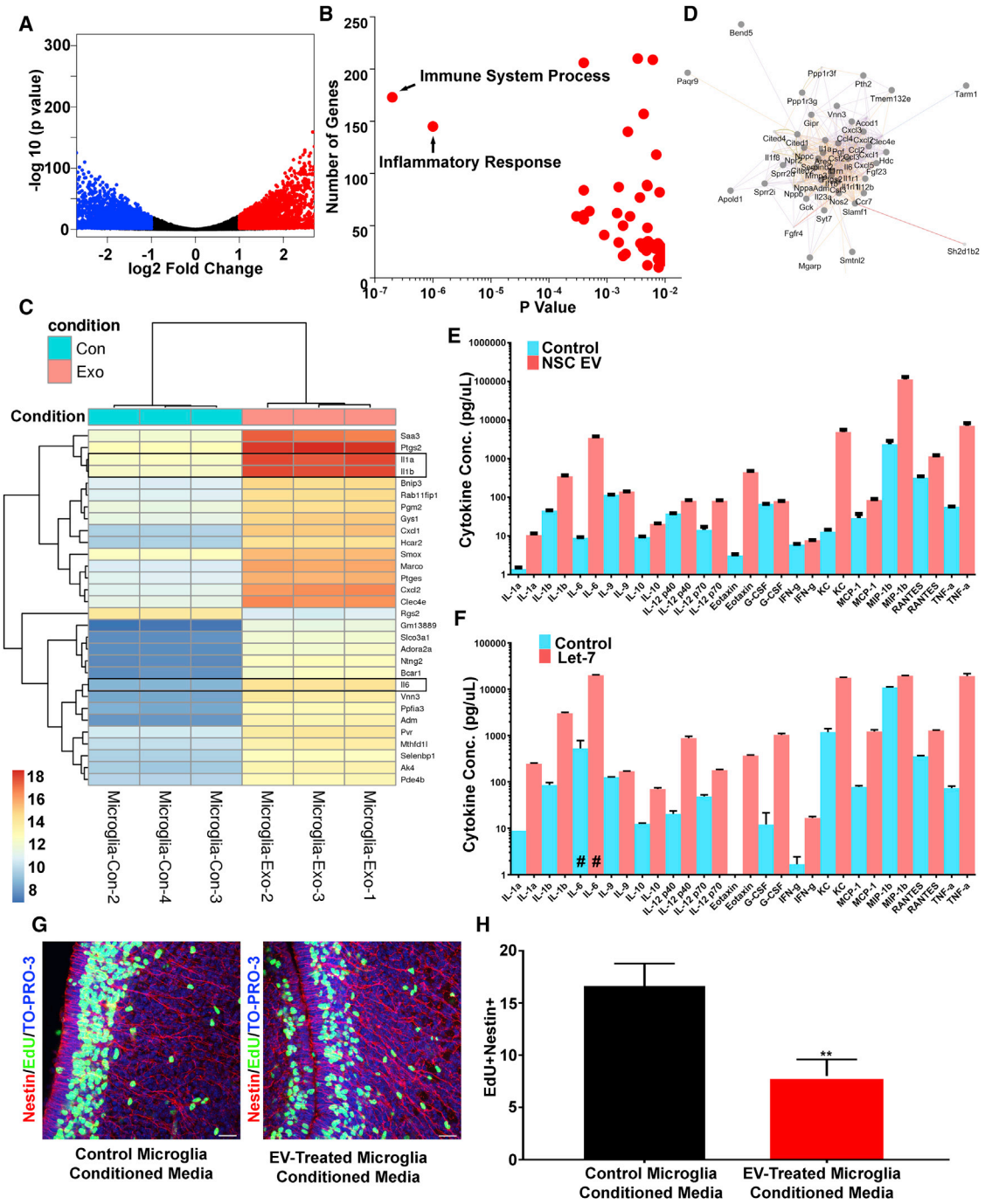

Figure 5. NSC EVs Activate a Microglia Transcriptional Network, Resulting in an NSC Feedback Loop

(A) Volcano plot of p values and fold changes of microglia mRNAs after NSC EV treatment.

(B) Gene ontology terms represented by p value and number of genes changed in the microglia gene network.

(C) Bi-clustering heatmap of the top 30 significantly altered mRNAs from control or NSC EV-treated microglia.

(D) Gene network analysis of the top differentially expressed microglia mRNAs demonstrates clustering of cytokines and cytokine receptors.

(E) Cytokine levels in medium from control and NSC EV-treated microglia.

(F) Cytokine levels from microglia-conditioned medium from N2a control and synthetic Let-7 transfected exosomes. #, = fluorescence.

(G) Representative images of brains injected with control or NSC EV microglia-conditioned medium, Edu-labeled (green), subjected to immunohistochemistry for Nestin (red), and counterstained with TO-PRO-3 (blue). Scale bar, 25 μm.

(H) Quantification of the percentage of EdU-positive, Nestin-positive neural stem cells.

See also Figure S2. Data are represented as mean ± SEM. **p < 0.01.

such as neuroblast delamination from the ventricular surface (Das and Storey, 2014). Therefore, SVZ NSC EVs represent another member of the ever-increasing developmental EV repertoire.

An age-dependent decrease in the number of extracellular CD9-GFP-positive particles was identified that coincided with the influx of microglia. Using an unbiased approach of labeling EVs, we found that EVs target microglia, as indicated by the markers Iba1, CD11b, and CD68. Iba1-positive cells accounted for the majority of DiI-labeled cells. The mechanism involved in the selectivity of uptake is unclear. Nevertheless, oligodendrocyte and glioma exosomes are reported to be taken up by microglia (Fitzner et al., 2011; van der Vos et al., 2016). Because EV content is proposed to contain encoded information, next-generation small RNA sequencing was performed and identified several miRNAs, including miR-9, Let-7, and miR-181 members. The presence of these regulatory miRNAs evoked us to hypothesize that EVs may function as a non-canonical morphogen. Consistent with this finding, EV uptake was associated with a shift to a reduced number of cellular processes and a rounded appearance as well as an accumulation within the SVZ. We cannot rule out the possibility that non-nucleic acid components contribute to the effect of EVs on microglia, nor can a nutritive role for EVs be excluded. Nevertheless, these findings establish relevance for NSC EVs on microglia in the neonatal brain.

NSC EVs had a direct effect on microglia in primary culture. The uptake of EVs resulted in a robust re-wiring of transcriptional networks, most notably those associated with immune system gene ontology terms, including immune system process, inflammatory response, defense response to virus, neutrophil chemotaxis, positive regulation of cytokine secretion, and I-kappa B kinase/nuclear factor κB (NF-κB) signaling. Transcriptional changes corresponded to enhanced cytokine release, most notably IL-6 and tumor necrosis factor alpha (TNF-α). Although the precise molecular mechanism by which EVs stimulate this response is unclear, levels of Let-7 family members altered the extent of cytokine release. It is possible that NSC EVs and Let-7 function as pattern recognition signals. In this case, during development, NSC EVs function as a morphogen-associated molecular pattern to control microglia. To determine the physiological effects of this signal, conditioned medium from microglia was injected into the lateral ventricles of mice. Conditioned medium from exosome-treated microglia regulated NSC proliferation. The effect of microglia-conditioned medium on NSCs is consistent with microglia regulation of dentate gyrus and embryonic ventricular zone NSCs (Cunningham et al., 2013; Gebara et al., 2013).

In conclusion, the results of this study demonstrate that SVZ NSCs release EVs that are selectively targeted to and functionally affect microglia. These results compel us to propose a conciliatory model of EV function that explains the discrepancy between EVs carrying refuse and information. In the case of neonatal development, NSC EVs function as a non-canonical morphogen that affects the state, organization, and morphology of microglia in the brain. It is therefore not surprising that EVs are associated with both normal neurodevelopment and a range of neurological disorders.

EXPERIMENTAL PROCEDURES

Animals

Experiments were performed according to guidelines set forth by the Clemson University Institutional Animal Care and Use Committee and NIH Guide for the Care and Use of Laboratory Animals. Pregnant CD-1 mice obtained from Charles River Laboratories were housed under pathogen-free conditions with a 12-hr light/dark cycle. For primary cell culture, EV and exosome preparation, and sequencing, pooled samples of both genders were used.

Electroporation

Electroporations were performed as described previously (Feliciano et al., 2013). Briefly, DNA combined with fast green was injected into the lateral ventricle. Pups were electroporated with a BTX ECM 830 Square Wave Pulse generator and Tweezertrodes (Harvard Apparatus).

Slice Preparation and Immunohistochemistry

Slices were prepared as described previously (Feliciano et al., 2011). Antibodies used included Nestin (Novus Biologicals, NB100-1604), CD9 (eBioscience, 14-0091-81), Iba1 (Novus, NB100-2833), CD68 (Bio-Rad, MCA1957), CD11b (Bio-Rad, MCA711G), or GFAP (Cell Signaling Technology, 12389S). Secondary antibodies conjugated to Alexa Fluor 488 or Alexa Fluor 633 (Life Technologies) were incubated overnight at 4°C.

Imaging

Images were taken on a Leica TCS SPE spectral confocal microscope using 20×, 40×, or 63× oil immersion lenses. Images were processed using Leica Application Suite X software (Leica Microsystems).

Exosome Isolation

Supernatant was collected and centrifuged at 300 × *g* for 10 min and 2,000 × *g* for 10 min, followed by 100,000 × *g* centrifugation in a Beckman Coulter Optima MAX-XP with a TLA 100.3 rotor for 90 min (P100 fraction). EVs were then subjected to further purification via sucrose density gradients consisting of 8%, 30%, 45%, and 60% layers in PBS and centrifuged at 232,000 × *g* for 30 min to 18 hr at 4°C. 10 fractions were collected, diluted 1:10 in PBS, and centrifuged for 1 hr at 100,000 × *g*. Each fraction was re-suspended in 4× Laemmli buffer and subjected to western blotting or PBS for further analysis. For exosome transfection experiments, P100 fractions were resuspended in 2.5 M sucrose, and density gradients were constructed from 2.5 M to 0.25 M (2.5 M, 2 M, 1.5 M, 1 M, 0.5 M, and 0.25 M). Gradients were centrifuged at 100,000 × *g* for 18 hr at 4°C. 10 Fractions were collected and diluted 1:10 in PBS and centrifuged for 1 hr at 100,000 × *g* at 4°C. Fractions were resuspended in Dulbecco's PBS and stored at –20°C.

Electron Microscopy

EVs suspended in 4% paraformaldehyde were embedded in a formvar carbon-coated grid, washed in PBS, fixed in 1% glutaraldehyde, and stained with saturated aqueous uranyl oxalate. EVs were embedded in 0.4% w/v uranyl acetate and 1.8% w/v methylcellulose. Samples were imaged with a Carl Zeiss 910 electron microscope (Carl Zeiss Microscopy, Thornwood, NY).

Neonatal Transplantation and Click-iT EdU Labeling

DiI-labeled P100 fractions were preloaded into capillary tubes and loaded with 2 μL of EV/DiI/PBS mixture, and EVs were injected into the lateral ventricle. Pups were placed onto a heating pad for 5 min until recovered and placed back into cages. Medium collected from cultured microglia was loaded into capillary tubes, and approximately 2 μL of medium was transplanted into the lateral ventricles of P0 pups. The Click-iT EdU imaging kit (Invitrogen, C10338) was used according to the manufacturer's protocol to assess proliferation.

DiI Labeling of P100 Fractions

P100 fractions were isolated as described above. P100 fractions were centrifuged at 14,000 × *g* for 30 min. Pellets were re-suspended in PBS and subjected to DiI labeling (1:1,000 at room temperature [RT], Life Technologies, V22889) for 10 min while vortexing periodically during incubation. DiI-labeled

P100 fractions were centrifuged at 14,000 × *g* for 30 min and re-suspended in 1× PBS. Centrifugation was repeated a total of three times. The final pellet was re-suspended in 50 μL 1× PBS and stored at –20°C.

Western Blot

Samples were lysed in radioimmunoprecipitation assay (RIPA) buffer, 2% SDS, and Halt protease and phosphatase inhibitor cocktail (Thermo Fisher Scientific). Samples were placed on ice, sonicated with a Q55 sonicator (QSonica), and centrifuged, and the supernatant was placed into fresh tubes. The following antibodies were used: CD63 (1:1,000, System Biosciences), CD9 (1:1,000, System Biosciences), ALIX (3A9, 1:1,000, Cell Signaling Technology, 21711), β-tubulin III (Aves Labs, TUJ), or His tag (D3I1O, 1:1,000, Cell Signaling Technology, 12698). Horseradish peroxidase (HRP)-conjugated antibodies from Life Technologies were used as a secondary antibody (1:3,333–1:5,000). polyvinylidene fluoride (PVDF) membranes were incubated with ECL substrate (Pierce) and exposed to Amersham Hyperfilm ECL (GE Healthcare).

Primary Neural Stem Cell Culture and Immunocytochemistry

The protocol was derived from Walker and Kempermann (2014). Cells were cultured in 500 μL Neurobasal A complete medium (1× Glutamax, 50 units/mL penicillin/streptomycin, 20 ng/mL epidermal growth factor (EGF), 20 ng/mL fibroblast growth factor 2 (FGF-2), and 2% B27 Supplement). Cells were placed on laminin-coated plates or coverslips in 24-well plates in Neurobasal A complete medium. The following day, complete media was refreshed, and the supernatant was stored at –20°C.

24 hr later, culture medium was collected and used for exosome and P100 isolation. Cells were lysed with 1× RIPA, 2% SDS, and PBS and used for western blotting or fixed by adding equal volumes of 37°C fixative solution (4% paraformaldehyde in 300 mM sucrose and Neurobasal A) directly to the wells and incubated at 37°C for 10 min. Coverslips were then washed three times, blocked in antibody buffer (PBS, 2% BSA, and 0.1% Tween 20) with 0.1% Triton X-100 and then washed again three times. Coverslips were incubated with antibodies against anti-CD9 mouse (eBioscience, 1:1,000), Nestin (Novus, 1:1,000), Iba1 (Vector Laboratories, VP-RM04, 1:500), and DCX (Santa Cruz Biotechnology, C-18, 1:500), washed three times, and then incubated in antibody buffer with the appropriate secondary antibodies (1:1,000, Life Technologies). Following four 15-min washes, coverslips were mounted in ProLong Gold Antifade with DAPI (Life Technologies) on Superfrost microscope slides (Thermo Scientific).

Analysis: Distribution

Co-localization and distribution of CD9-GFP in electroporated postnatal neural stem cells were analyzed using Fiji. z stack images were loaded into Fiji software, Z-projected (Max Intensity), and separated from stacks to images based on fluorescent channels (i.e., green, red, or blue). Brightness/contrast was adjusted for each Z-projected image to reduce background noise. Using the Co-localization plugin in Fiji, Z-projected images were assessed for co-localization of CD9-GFP and Tomato. The co-localization threshold of each image was set between 85–130 using 5-point increments when adjusting. Images were subjected to particle analysis through the Analyze Particle plugin. Green particle size was set from 1 micron to infinity to detect small CD9-GFP particles, and Tomato particle size was set from 10 microns to infinity to only count the number of cells and not cell debris. The percentage of CD9-GFP and Tomato co-localization was recorded.

DiI and Cell Type Co-localization (Iba1, CD11b, and CD68)

Images were loaded into Fiji (ImageJ) and converted into composite images. Z sections were selected based on DiI and Iba1/CD11b/CD68 co-localization within the selected Z section. Selected sections were Z-projected using max project and separated into individual color channels. Brightness and contrast were adjusted to correct for background noise within each image. Co-localization analysis was performed on Z-projected DiI and Iba1/CD11b/CD68 images. Co-localized images were converted to 8 bits, inverted, and thresholded to 0 and 255 (only co-localized particles were visible). Thresholds of Z-projected DiI and Iba1/CD11b/CD68 images were set to 10/255 and 85–100/255, respectively. All images were then subjected to particle analysis. The percentage of co-localized DiI particles was in relation to the total number of DiI particles.

Morphological Analysis: Ellipticity and Process Number

Cellular ellipticity was measured using Shape Description in Particle Analysis in ImageJ. Images were loaded into ImageJ, Z-projected, and separated into individual channels (green, red, and blue). Thresholds were set at 100–120 and 255. Cells either in the SVZ or in the ventricular wall were outlined using the freehand tool and assessed through particle analysis. Circularity was reported as a value between 0 and 1, with 1 describing a perfect circle. Microglia complexity analysis was conducted using Leica Application Suite X (LASx) 1.1.0.12420 3D module software. Processes of Iba1+ cells were quantified manually in the 3D module. The average number of processes in DiI+/Iba1+ cells was compared with DiI-/Iba1+ cells.

Nanosight Particle Tracking Analysis

Samples were shipped on wet ice to the Nanomedicine Characterization Core facility in the Center for Nanotechnology in Drug Delivery at the University of North Carolina (UNC) at Chapel Hill. Samples were prepared in a laminar flow hood and thawed at RT. Sample dilutions were based on an initial run with PBS, 10 mM salt. Samples were loaded onto a pre-cleaned and pre-warmed Nanosight NS 500 nanoparticle characterization system (NanoSight, UK) equipped with a 532-nm laser and a 565-nm long pass filter. Mean size and particle concentration values were calculated by the nanoparticle tracking software. The Nanosight NS 500 was calibrated with 100 nm polystyrene latex microsphere standards (Nanosight, UK), and readings were acquired at 23.3°C.

RNA Sequencing

For EV small RNA sequencing, RNA was isolated by Trizol extraction from EVs from P100 fractions of primary SVZ NSCs. Samples were quantified using the Agilent Bioanalyzer small RNA assay. Libraries were prepared according to manufacturer's protocol (Illumina small RNA preparation kit). Samples were subjected to 1 × 75 bp single-end reads at an approximate depth of 10–15 million reads per sample on an Illumina Hi-Seq.

RNA was isolated from microglia cell cultures using Trizol in accordance with the manufacturer's protocol. Three samples from 1–2 RNA isolations for each condition were used to generate libraries. RNA concentrations and purity were assessed by Nanodrop, Qubit assay, and Agilent Tapestation. RNA library preparation with poly(A) selection was performed using the NEBNext Ultra RNA Library Preparation Kit according to the manufacturer's protocol (New England Biolabs). 2 × 150 bp reads were generated at a depth of 56–84 million reads per sample on an Illumina HiSeq. Samples had a mean quality score of 38.52, with 92.76% of bases having a ≥ Q30 score. Sequence reads were trimmed to remove possible adaptor sequences and nucleotides with poor quality using Trimmomatic v0.36. The reads were then mapped to the *Mus musculus* GRCm38 reference genome available on ENSEMBL using the STAR aligner. The RNA sequencing (RNA-seq) aligner is executed using a splice aligner that detects splice junctions and incorporating them to help align the entire read sequences. Unique exon hit counts were calculated using feature counts from the Subread package. After mapping and unique exon hit count calculations, downstream differential expression analysis was performed using DESeq2. Gene ontology (GO) analysis was performed on the statistically significant set of genes by implementing the software GeneSCF. The Mouse Genome Informatics GO list was used to cluster the set of genes based on their biological process and determine their statistical significance. Gene interaction networks were determined by Cytoscape 3.60 using Genemania.

Luminex

Cytokine concentrations were quantified with the cytokine multiplex assay from Bio-Rad as described previously (Racicot et al., 2017). Wells of a 96-well filter plate were loaded with 50 μL of prepared standard solution or 50 μL of cell-free supernatant and incubated with the Bio-Plex Pro mouse 23-plex assay from Bio-Rad at ± 800 rpm for 30 min in the dark at RT. Wells were vacuum-washed three times with 100 μL wash buffer. Samples were then incubated with 25 μL of biotinylated detection antibody at ± 800 rpm

for 30 min at RT in the dark. After three washes, 50 μL of streptavidin-phycoerythrin was added to each well and incubated for 10 min at ± 800 rpm at RT in the dark. After a final wash, the beads were resuspended in 125 μL of sheath buffer for measurement with the Luminex 200 (Luminex, Austin, TX)

Microglia Culture

24 hr prior to plating microglia, 6 well plates were coated with 10 μg/mL poly-L-lysine according to the supplier's instructions. The protocol was derived from Bohlen et al. (2017). Primary microglia cells isolated from CD1 mice were reconstituted in a 37°C water bath immediately prior to plating. For immunohistochemistry following exosome treatment experiments, 3,500 cells were plated in 500 μL microglia complete medium (2 ng/mL TGF-β2, 100 ng/mL IL-34, 1.5 mg/mL cholesterol, 100 units/mL penicillin-streptomycin [pen-strep], 1× Glutamax, and microglia medium [Sciencell, 1901]) and allowed to adhere for 10 min at RT in 24-well plates.

Exo-fection

After sucrose density gradient isolation of Neuro-2a exosomes or extracellular vesicles, the respective vesicles were transfected (System Biosciences, EXFT10A-1). In brief, isolated vesicles were mixed with 10 μL Exo-Fect solution, synthetic Let-7 miRNAs (Sigma; HMI0007, HMI0009, and HMI0017, which also correspond to mouse Let-7), and Dulbecco's phosphate-buffered saline (dPBS). Tubes were incubated at 37°C for 10 min then immediately placed on ice. Samples were centrifuged at 14,000 x g for 15 min at 4°C. Samples were either used to treated cultured primary microglia or labeled with DiI and injected into the lateral ventricles of P0 pups as described previously.

Statistics

Statistics were performed with Prism software (version 6; GraphPad). Significance was calculated using unpaired t tests and one-way ANOVA with Tukey's multiple comparisons test. Statistical significance was defined as $p < 0.05$. All data are presented as mean ± SEM. The Wald test, p values, and absolute Log_2Fold changes were generated for gene expression analysis. Genes with adjusted $p < 0.05$ and absolute Log_2Fold change > 2 were called as differentially expressed genes for each comparison.

DATA AND SOFTWARE AVAILABILITY

The accession number for the RNA sequencing data reported in this paper is GEO: GSE110892.

SUPPLEMENTAL INFORMATION

Supplemental Information includes Supplemental Experimental Procedures and two figures and can be found with this article online at https://doi.org/10.1016/j.celrep.2018.03.037.

ACKNOWLEDGMENTS

David M. Feliciano is supported by grants from the Whitehall Foundation (2015-08-05) and the NIH (1R15NS096562). We thank Dr. Angelique Bordey for providing Tomato plasmids. We thank Joseph Caruso for technical assistance. We thank Dr. Matthew J. Haney of the Nanomedicine Characterization core facility at the Center for Nanotechnology in Drug Delivery at the University of North Carolina, Chapel Hill. We thank Sue Ann Mentone of the Department of Cellular and Molecular Physiology, Yale University School of Medicine, for expertise in electron microscopy. We thank Paulomi Aldo and Dr. Gil Mor of the Department of Obstetrics, Gynecology, and Reproductive Sciences at Yale University for assistance with Luminex assays.

AUTHOR CONTRIBUTIONS

Conceptualization, D.M.F.; Methodology, D.M.F. and M.C.M.; Validation, D.M.F., M.C.M., C.M.S., J.C.H., and V.N.N.; Formal Analysis, M.C.M.; Investigation, M.C.M., V.N.N., D.M.F., J.C.H., and C.M.S.; Writing – Original Draft, D.M.F.; Writing – Review & Editing, D.M.F. and M.C.M.; Visualization, M.C.M. and D.M.F. Supervision, D.M.F.; Project Administration, D.M.F., M.C.M., and J.C.H.; Funding Acquisition, D.M.F.

DECLARATION OF INTERESTS

The authors declare no competing financial interests.

Received: August 17, 2017
Revised: February 19, 2018
Accepted: March 9, 2018
Published: April 3, 2018

REFERENCES

Alliot, F., Lecain, E., Grima, B., and Pessac, B. (1991). Microglial progenitors with a high proliferative potential in the embryonic and adult mouse brain. Proc. Natl. Acad. Sci. USA *88*, 1541–1545.

Alliot, F., Godin, I., and Pessac, B. (1999). Microglia derive from progenitors, originating from the yolk sac, and which proliferate in the brain. Brain Res. Dev. Brain Res. *117*, 145–152.

Bohlen, C.J., Bennett, F.C., Tucker, A.F., Collins, H.Y., Mulinyawe, S.B., and Barres, B.A. (2017). Diverse Requirements for Microglial Survival, Specification, and Function Revealed by Defined-Medium Cultures. Neuron *94*, 759–773.e8.

Choe, Y., Pleasure, S.J., and Mira, H. (2015). Control of Adult Neurogenesis by Short-Range Morphogenic-Signaling Molecules. Cold Spring Harb. Perspect. Biol. *8*, a018887.

Cocucci, E., and Meldolesi, J. (2015). Ectosomes and exosomes: shedding the confusion between extracellular vesicles. Trends Cell Biol. *25*, 364–372.

Cossetti, C., Iraci, N., Mercer, T.R., Leonardi, T., Alpi, E., Drago, D., Alfaro-Cervello, C., Saini, H.K., Davis, M.P., Schaeffer, J., et al. (2014). Extracellular vesicles from neural stem cells transfer IFN-γ via Ifngr1 to activate Stat1 signaling in target cells. Mol. Cell *56*, 193–204.

Cunningham, C.L., Martínez-Cerdeño, V., and Noctor, S.C. (2013). Microglia regulate the number of neural precursor cells in the developing cerebral cortex. J. Neurosci. *33*, 4216–4233.

Das, R.M., and Storey, K.G. (2014). Apical abscission alters cell polarity and dismantles the primary cilium during neurogenesis. Science *343*, 200–204.

Dietrich, J., Imitola, J., and Kesari, S. (2008). Mechanisms of Disease: the role of stem cells in the biology and treatment of gliomas. Nat. Clin. Pract. Oncol. *5*, 393–404.

Feliciano, D.M., Lafourcade, C.A., and Bordey, A. (2013). Neonatal subventricular zone electroporation. J. Vis. Exp. *72*, 50197.

Feliciano, D.M., Su, T., Lopez, J., Platel, J.C., and Bordey, A. (2011). Single-cell Tsc1 knockout during corticogenesis generates tuber-like lesions and reduces seizure threshold in mice. J. Clin. Invest. *121*, 1596–1607.

Feliciano, D.M., Zhang, S., Nasrallah, C.M., Lisgo, S.N., and Bordey, A. (2014). Embryonic cerebrospinal fluid nanovesicles carry evolutionarily conserved molecules and promote neural stem cell amplification. PLoS ONE *9*, e88810.

Fitzner, D., Schnaars, M., van Rossum, D., Krishnamoorthy, G., Dibaj, P., Bakhti, M., Regen, T., Hanisch, U.K., and Simons, M. (2011). Selective transfer of exosomes from oligodendrocytes to microglia by macropinocytosis. J. Cell Sci. *124*, 447–458.

Gebara, E., Sultan, S., Kocher-Braissant, J., and Toni, N. (2013). Adult hippocampal neurogenesis inversely correlates with microglia in conditions of voluntary running and aging. Front. Neurosci. *7*, 145.

Ginhoux, F., Greter, M., Leboeuf, M., Nandi, S., See, P., Gokhan, S., Mehler, M.F., Conway, S.J., Ng, L.G., Stanley, E.R., et al. (2010). Fate mapping analysis reveals that adult microglia derive from primitive macrophages. Science *330*, 841–845.

Henry, A.M., and Hohmann, J.G. (2012). High-resolution gene expression atlases for adult and developing mouse brain and spinal cord. Mamm. Genome *23*, 539–549.

Iraci, N., Gaude, E., Leonardi, T., Costa, A.S.H., Cossetti, C., Peruzzotti-Jametti, L., Bernstock, J.D., Saini, H.K., Gelati, M., Vescovi, A.L., et al. (2017). Extracellular vesicles are independent metabolic units with asparaginase activity. Nat. Chem. Biol. *13*, 951–955.

Karlsson, G., Rörby, E., Pina, C., Soneji, S., Reckzeh, K., Miharada, K., Karlsson, C., Guo, Y., Fugazza, C., Gupta, R., et al. (2013). The tetraspanin CD9 affords high-purity capture of all murine hematopoietic stem cells. Cell Rep. *4*, 642–648.

Kolle, G., Ho, M., Zhou, Q., Chy, H.S., Krishnan, K., Cloonan, N., Bertoncello, I., Laslett, A.L., and Grimmond, S.M. (2009). Identification of human embryonic stem cell surface markers by combined membrane-polysome translation state array analysis and immunotranscriptional profiling. Stem Cells *27*, 2446–2456.

Kumar, A., Bhatia, H.S., de Oliveira, A.C., and Fiebich, B.L. (2015). microRNA-26a modulates inflammatory response induced by toll-like receptor 4 stimulation in microglia. J. Neurochem. *135*, 1189–1202.

Lehmann, S.M., Krüger, C., Park, B., Derkow, K., Rosenberger, K., Baumgart, J., Trimbuch, T., Eom, G., Hinz, M., Kaul, D., et al. (2012). An unconventional role for miRNA: let-7 activates Toll-like receptor 7 and causes neurodegeneration. Nat. Neurosci. *15*, 827–835.

Leung, K.T., Chan, K.Y., Ng, P.C., Lau, T.K., Chiu, W.M., Tsang, K.S., Li, C.K., Kong, C.K., and Li, K. (2011). The tetraspanin CD9 regulates migration, adhesion, and homing of human cord blood CD34+ hematopoietic stem and progenitor cells. Blood *117*, 1840–1850.

Lim, D.A., and Alvarez-Buylla, A. (2016). The Adult Ventricular-Subventricular Zone (V-SVZ) and Olfactory Bulb (OB) Neurogenesis. Cold Spring Harb. Perspect. Biol. *8*, a018820.

Lledo, P.M., and Valley, M. (2016). Adult Olfactory Bulb Neurogenesis. Cold Spring Harb. Perspect. Biol. *8*, a018945.

Llorens-Bobadilla, E., Zhao, S., Baser, A., Saiz-Castro, G., Zwadlo, K., and Martin-Villalba, A. (2015). Single-Cell Transcriptomics Reveals a Population of Dormant Neural Stem Cells that Become Activated upon Brain Injury. Cell Stem Cell *17*, 329–340.

Morton, M.C., and Feliciano, D.M. (2016). Neurovesicles in Brain Development. Cell. Mol. Neurobiol. *36*, 409–416.

Nimmerjahn, A., Kirchhoff, F., and Helmchen, F. (2005). Resting microglial cells are highly dynamic surveillants of brain parenchyma in vivo. Science *308*, 1314–1318.

Oka, M., Tagoku, K., Russell, T.L., Nakano, Y., Hamazaki, T., Meyer, E.M., Yokota, T., and Terada, N. (2002). CD9 is associated with leukemia inhibitory factor-mediated maintenance of embryonic stem cells. Mol. Biol. Cell *13*, 1274–1281.

Pluchino, S., and Cossetti, C. (2013). How stem cells speak with host immune cells in inflammatory brain diseases. Glia *61*, 1379–1401.

Prinz, M., Erny, D., and Hagemeyer, N. (2017). Ontogeny and homeostasis of CNS myeloid cells. Nat. Immunol. *18*, 385–392.

Racicot, K., Aldo, P., El-Guindy, A., Kwon, J.Y., Romero, R., and Mor, G. (2017). Cutting edge: Fetal/placental type I IFN can affect maternal survival and fetal viral load during viral infection. J. Immunol. *198*, 3029–3032.

Raposo, G., and Stoorvogel, W. (2013). Extracellular vesicles: exosomes, microvesicles, and friends. J. Cell Biol. *200*, 373–383.

Sato, K. (2015). Effects of Microglia on Neurogenesis. Glia *63*, 1394–1405.

Shi, Y., Zhou, W., Cheng, L., Chen, C., Huang, Z., Fang, X., Wu, Q., He, Z., Xu, S., Lathia, J.D., et al. (2017). Tetraspanin CD9 stabilizes gp130 by preventing its ubiquitin-dependent lysosomal degradation to promote STAT3 activation in glioma stem cells. Cell Death Differ. *24*, 167–180.

Shigemoto-Mogami, Y., Hoshikawa, K., Goldman, J.E., Sekino, Y., and Sato, K. (2014). Microglia enhance neurogenesis and oligodendrogenesis in the early postnatal subventricular zone. J. Neurosci. *34*, 2231–2243.

Terada, N., Baracskay, K., Kinter, M., Melrose, S., Brophy, P.J., Boucheix, C., Bjartmar, C., Kidd, G., and Trapp, B.D. (2002). The tetraspanin protein, CD9, is expressed by progenitor cells committed to oligodendrogenesis and is linked to beta1 integrin, CD81, and Tspan-2. Glia *40*, 350–359.

Tietje, A., Maron, K.N., Wei, Y., and Feliciano, D.M. (2014). Cerebrospinal fluid extracellular vesicles undergo age dependent declines and contain known and novel non-coding RNAs. PLoS ONE *9*, e113116.

van der Vos, K.E., Abels, E.R., Zhang, X., Lai, C., Carrizosa, E., Oakley, D., Prabhakar, S., Mardini, O., Crommentuijn, M.H., Skog, J., et al. (2016). Directly visualized glioblastoma-derived extracellular vesicles transfer RNA to microglia/macrophages in the brain. Neuro-oncol. *18*, 58–69.

Vescovi, A.L., Galli, R., and Reynolds, B.A. (2006). Brain tumour stem cells. Nat. Rev. Cancer *6*, 425–436.

Walker, T.L., and Kempermann, G. (2014). One mouse, two cultures: isolation and culture of adult neural stem cells from the two neurogenic zones of individual mice. J. Vis. Exp. *84*, e51225.

Yao, H., Ma, R., Yang, L., Hu, G., Chen, X., Duan, M., Kook, Y., Niu, F., Liao, K., Fu, M., et al. (2014). MiR-9 promotes microglial activation by targeting MCPIP1. Nat. Commun. *5*, 4386.

Zhang, L., Li, Y.J., Wu, X.Y., Hong, Z., and Wei, W.S. (2015). MicroRNA-181c negatively regulates the inflammatory response in oxygen-glucose-deprived microglia by targeting Toll-like receptor 4. J. Neurochem. *132*, 713–723.

Zhang, Y., Kim, M.S., Jia, B., Yan, J., Zuniga-Hertz, J.P., Han, C., and Cai, D. (2017). Hypothalamic stem cells control ageing speed partly through exosomal miRNAs. Nature *548*, 52–57.

Zhou, J., Shrikhande, G., Xu, J., McKay, R.M., Burns, D.K., Johnson, J.E., and Parada, L.F. (2011). Tsc1 mutant neural stem/progenitor cells exhibit migration deficits and give rise to subependymal lesions in the lateral ventricle. Genes Dev. *25*, 1595–1600.